Robotica (2010) volume 28, pp. 135–148. © Cambridge University Press 2009
doi:10.1017/S0263574709005669

Optimal plane beams modelling elastic linear objects

Sung K. Koh and Guangjun Liu*

Department of Aerospace Engineering, Ryerson University, Toronto, ON M5B 2K3, Canada

(Received in Final Form: April 8, 2009. First published online: May 15, 2009)

SUMMARY

This paper discusses analytical and deterministic models for a plane curve with minimum deformation that may be utilized in planning the motion of elastic linear objects and investigating the inverse kinematics of a hyper-redundant robot. It usually requires intensive computation to determine the configuration of elastic linear objects. In addition, conventional optimization-based numerical techniques that identify the shape of elastic linear objects in equilibrium involve non-deterministic aspects. Several analytical models that produce the configuration of elastic linear objects in an efficient and deterministic manner are presented in this paper. To develop the analytical expressions for elastic linear objects, we consider a cantilever beam where the deflections are determined according to the Euler–Bernoulli beam theory. The deflections of the cantilever beam are determined for prescribed constraints imposed on the deflections at the free end to replicate various elastic linear objects. Deflections of a cantilever beam with roller supports are explored to replicate elastic linear objects in contact with rigid objects. We verify the analytical models by comparing them with exact beam deflections. The analytical model is precisely accurate for beams with small deflections as it is developed on the basis of the Euler–Bernoulli beam theory. Although it is applied to beams undergoing large deflections, it is still reasonably accurate and at least as precise as the conventional pseudo-rigid-body model. The computational demand involved in using the analytical models is negligible. Therefore, efficient motion planning for elastic linear objects can be realized when the proposed analytical models are combined with conventional motion planning algorithms. We also demonstrate that the analytical model solves the inverse kinematics problem in an efficient and robust manner through numerical simulations.

KEYWORDS: Elastic linear objects; Euler–Bernoulli beam theory; Elasticity theory; Hyper-redundant robots; Motion planning; Inverse kinematics.

1. Introduction

The kinematics of flexible systems has been of interest to many researchers for decades because it is of importance in planning the motion of flexible systems such as hyper-redundant robots, cables, elastic sheets and sutures. To understand the kinematics of flexible systems, there is a need to replicate their kinematics using reasonably accurate and simple models. The focus of this paper is to develop deterministic, efficient and reasonably accurate models for flexible systems based on the analogy between flexible systems with minimum deformation and elastic systems in equilibrium. Configurations with minimum deformation are always preferred in designing the motion of flexible systems. If the system does not have minimum deformation, additional energy is required for the system to achieve the configuration. It is a challenging task to model flexible systems because they can take on an infinite number of feasible configurations and a number of degrees of freedom are required to describe their configurations.

In this paper, we are concerned with extensible or inextensible flexible plane curves that have minimum deformations. Since the deformations occur on a two-dimensional plane, the plane curves are defined only by the curvature.[10,15] The deformation of a plane curve of length l is measured by the curvature energy defined as follows:

$$\mathrm{CE} = \int_0^l \kappa(s)^2 \, \mathrm{d}\, s, \tag{1}$$

where s denotes the coordinate along the curve and κ refers to the curvature at s. We refer to optimal plane curves as those with minimum curvature energy. The optimal path between two given configurations consists of optimal curves.

The motivation for this research stems from the need to understand the kinematics of flexible systems such as a cable, an elastic sheet or a hyper-redundant robot for their motion planning. Hyper-redundant robots are often modelled as flexible curves to solve the inverse kinematics problem.[3,29] The configurations of the hyper-redundant robot with a specific end-effector configuration are acquired from the curves with equivalent endpoint configurations. There are several fitting techniques for approximating a continuous curve with a piecewise linear one, which enables determining the configuration of a hyper-redundant robot for a given desired curve.[1,7] Unfortunately, conventional computational techniques that determine optimal curves require intensive computation and involve non-deterministic aspects. It is important to establish an efficient and deterministic means of predicting the behaviour of elastic linear objects in order to realize practical motion planning for flexible systems and hyper-redundant robots. In this paper, we aim to develop simple analytical models for elastic linear objects in a two-dimensional space that provide the configurations in equilibrium in an efficient and deterministic manner. Although it is desirable to develop

* Corresponding author. E-mail: gjliu@ryerson.ca

an analytical model for spatial curves with minimum deformation, one can hardly take an analytical approach to the modelling due to the high degree of complexity involved in dealing with three-dimensional curves. Since no extensive analytical models have been developed even for general plane curves with minimum deformation, it still requires intensive computation to determine optimal spatial curves if one employ conventional computational techniques. The analytical model proposed in this paper will produce plane curves with minimum deformation without expensive computation, and hence is useful in planning the motion of hyper-redundant robots manipulated on a plane and identifying their configurations for a given end-effector configuration in a practical and efficient manner. We can also explore the kinematics of various flexible systems operated in a two-dimensional world on the basis of the analytical models. Elastic systems, such as a cable or an elastic sheet, can be modelled as an elastic linear object of constant length.

There is a large body of literature on flexible curves with minimum deformations. Horn[10] developed an analytical expression that approximates extensible plane curves with minimum curvature energy. Kallay[15] derived a set of non-linear equations that govern optimal plane curves of constant length with a specific endpoint constraint. Kallay[18] also proposed an intuitive iterative method that approximates an inextensible optimal curve with specific endpoint configurations. Chirikjian and Burdick[3] modelled a hyper-redundant robot as an extensible flexible curve and developed a Jacobian-based method that determines an extensible curve with minimum deformation energy for a particular set of boundary conditions. Wakamatsu and Hirai[27] parameterized a spatial curve using four shape-functions and formulated an unconstrained optimization problem to determine optimal curves. Based on this work, Wakamatsu *et al.*[28] proposed a path planning technique for knotting/unknotting of linear flexible objects using their topological representations. Ladd and Kavraki[13] applied motion planning techniques to find a sequence of motion to untangle mathematical knots. Moll and Kavraki[21] developed a subdivision scheme that determines a spatial curve with minimum strain energy. The strain energy of a curve in a three-dimensional space takes into account both the curvature and the torsion of the curve. Moll and Kavraki[21] represented a spatial curve as a sequence of segments with constant curvature and torsion, and minimized the curve strain energy by subdividing each segment in a way that the strain energy of each segment decreases. Kim and Chirikjian[18] derived differential equations for a spatial curve with minimum deformation in order to investigate the stable conformations of DNA. The differential equations were derived from the stationary condition of the Lagrangian defined for a three-dimensional elastic rod with minimum deformation and solved through an iterative procedure. An analytical expression for symmetric elastic rods was developed by Coleman *et al.*[5] and Swigon *et al.*[25] on the basis of the theory of Kirchhoff in order to examine the effects of geometric conditions imposed at the endpoints of DNA loops that have a symmetric configuration and parallel endpoints.

In spite of the significant progress that has been made in this area, the conventional approaches possess the following common drawbacks: (1) there are no analytical expressions for general optimal curves including asymmetric curves of constant length; (2) although several promising numerical techniques have been proposed,[3,9,16,19,21,27] the conventional computational approaches usually entail intensive computation; and (3) the conventional optimization-based numerical approach involves non-deterministic aspects.[12,23] One needs to solve either a constrained or an unconstrained optimization problem to compute optimal curves. As a result, it is difficult to determine the optimal curves unless one has information on the optimal solution prior to the optimization. It is also a challenging task to acquire the solutions to the differential equations for optimal spatial curves in a deterministic manner.[15,18] Finally, the feasibility of the endpoint constraints has never been discussed. Given the length of a curve and the configuration at the endpoint, it is not apparent whether the prescribed endpoint configuration can be achieved without the elongation of the curve.

In order to develop a simple analytical model for plane curves with minimum curvature energy, we are concerned with an elastic linear object with zero slope at one of the endpoints. Then various configurations of plane curves can be determined for a variety of constraints imposed on the position and slope at the other endpoint. Consequently, the problem under consideration is analogous to determining the deflections of a cantilever beam for prescribed boundary conditions at the free end. We derive analytical expressions for extensible optimal plane curves based on the Euler–Bernoulli beam theory.[6,8] The problems that will be addressed to establish the analytical models are as follows: First, given the position and slope at the endpoint and the length of a curve, we extract a plane optimal curve from an equivalent cantilever beam; secondly, elastic linear objects in contact with rigid objects will be determined from an equivalent cantilever beam with roller supports; and thirdly, for any given two optimal configurations, the motion of elastic linear objects will be planned using the optimal plane curves. We acquire the analytical expressions by solving a differential equation that governs elastic beams with small deflections. The analytical models are verified by comparing them with closed-form solutions developed for cantilever beams.[6,8,26] The accuracy of the analytical models is verified in comparison with a pseudo-rigid-body model.[11] The comparison with the pseudo-rigid-body model reveals that the analytical models are more accurate than the conventional pseudo-rigid-body model for beams with large deflections. Analytical models for a cantilever beam with roller support are also developed in order to represent elastic linear objects in contact with rigid objects. Finally, we demonstrate how the analytical models can be used in motion planning for elastic objects as a local path planner.

The remainder of this paper is divided into several sections as follows: In Section 2, an analytic expression for optimal plane curves is developed on the basis of the Euler–Bernoulli beam theory. In Section 3, the deflections of elastic beams with an overhang are evaluated in order to replicate elastic linear objects in contact with a rigid object. The proposed analytical model is generalized in order to represent elastic linear objects in contact with multiple rigid objects in Section 4. The proposed models are validated and their

https://doi.org/10.1017/S0263574709005669 Published online by Cambridge University Press

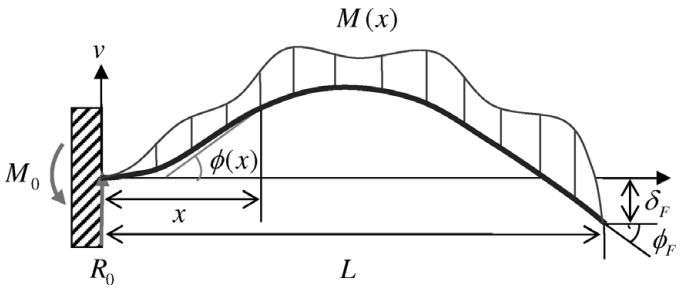

Fig. 1. A cantilever beam loaded by a distributed moment.

potential applications are investigated in Section 5. The contributions are summarized and concluding remarks are provided in the last section.

2. Analytical Model of Optimal Plane Curves

In this section, we develop a deterministic and analytical model for optimal plane curves based on the Euler–Bernoulli beam theory.[6,8]

A plane curve is modelled as the cantilever beam loaded by the distributed moment $M(x)$ shown in Fig. 1. In view of the Euler–Bernoulli beam theory, the bending moment $M_{\mathrm{b}}(x)$ developed by $M(x)$ is proportional to the rate of change of the slope ϕ along the beam

$$M_{\mathrm{b}}(x) = EI\frac{\mathrm{d}\phi}{\mathrm{d}x}, \tag{2}$$

where E is the elastic modulus of material and I is the second moment of area of the cross-sectional area. The rate of change of the slope, $\mathrm{d}\phi/\mathrm{d}x$, indicates the curvature. The curvature may be expressed in terms of the deflection $v(x)$ as follows:

$$\frac{\mathrm{d}\phi}{\mathrm{d}x} = \frac{\mathrm{d}^2v/\mathrm{d}x^2}{\left[1+(\mathrm{d}v/\mathrm{d}x)^2\right]^{3/2}}. \tag{3}$$

Note that no assumptions have been made in deriving Eq. (2). Hence, the solution to Eq. (2) describes the exact deflections of elastic beams. Closed-form solutions to Eq. (2) have been developed only for the beams subjected to simple loading and boundary conditions.[11]

When the deflections developed by external loads are small, the slope $\mathrm{d}v/\mathrm{d}x$ is small compared to unity; hence the term $(\mathrm{d}v/\mathrm{d}x)^2$ in Eq. (3) becomes negligible. Consequently, cantilever beams with small deflections are governed by the following linear differential equation that defines the relationship between the curvature $\mathrm{d}^2v/\mathrm{d}x^2$ and the bending moment $M_{\mathrm{b}}(x)$:

$$\frac{\mathrm{d}^2v}{\mathrm{d}x^2} = \frac{M_{\mathrm{b}}(x)}{EI}. \tag{4}$$

The differential equation (4) is referred to as the moment–curvature relationship. The small slope assumption is valid only when the beam undergoes small deflections, and hence the moment–curvature relationship predicts precisely accurate deflection curves for beams with small deflections. In addition, the Euler–Bernoulli beam model does not take into account angular deflections due to shear which are negligible when the deflections are small. The analytical model that will be developed in this section is acquired by solving the moment–curvature relationship for a generalized bending moment distribution. Therefore, the deflections estimated by the proposed model are accurate only for beams with small deflections. However, the computational demand involved in computing deflection curves using the analytical model is negligible. One may want to use the model depending on the degree of accuracy required in applying the model. Although the deflection estimated by the analytical model may not be precisely accurate for beams with large deflections, it still could be accurate enough depending on the application.

The deflection curve $v(x)$ is determined by integrating the linear differential equation (4) two times. Traditionally, the solution to Eq. (4) has been developed for certain loading conditions to acquire the deflection curve of a beam, whereas we are interested in identifying the loading condition that yields the deflection curve satisfying prescribed boundary conditions. The cantilever beam loaded by the distributed moment $M(x)$ in Fig. 1 is explored because such a loading condition can produce any feasible deflection curve. Consequently, we need to determine the distributed moment $M(x)$ that yields the deflection curve satisfying the prescribed vertical deflection δ_{F} and angular deflection ϕ_{F} at the free end.

In order to describe the bending moment $M_{\mathrm{b}}(x)$, developed by the distributed moment $M(x)$, in the most general manner, we make use of Fourier series that expresses the bending moment in terms of sine and cosine shape functions

$$M_{\mathrm{b}}(x) = a_0 + a_1\sin\left(\frac{2\pi x}{L}\right) + a_2\cos\left(\frac{2\pi x}{L}\right), \tag{5}$$

where L is the horizontal coordinate of the free end. We exclude higher-order terms in this series representation of the bending moment $M_b(x)$ in Eq. (5) because this is the simplest form of $M_{\mathrm{b}}(x)$ that can yield any feasible deflection curves for prescribed vertical and angular deflections at the free end as will be discussed later. The deflection is determined by solving the following differential equation, which is acquired by substituting Eq. (5) into Eq. (4):

$$EI\frac{\mathrm{d}^2v}{\mathrm{d}x^2} = a_0 + a_1\sin\left(\frac{2\pi x}{L}\right) + a_2\cos\left(\frac{2\pi x}{L}\right). \tag{6}$$

Integration of Eq. (6) leads to the angular deflection $\mathrm{d}v/\mathrm{d}x$ across the beam

$$EI\frac{\mathrm{d}v}{\mathrm{d}x} = a_0x - a_1\left(\frac{L}{2\pi}\right)\cos\left(\frac{2\pi x}{L}\right) + a_2\left(\frac{L}{2\pi}\right)\sin\left(\frac{2\pi x}{L}\right) + c_1, \tag{7}$$

where c_1 is the constant of integration. Integration of Eq. (7) yields the following deflection curve $v(x)$:

$$EIv = \frac{a_0}{2}x^2 - \left(\frac{a_1L^2}{4\pi^2}\right)\sin\left(\frac{2\pi x}{L}\right) - \left(\frac{a_2L^2}{4\pi^2}\right)\cos\left(\frac{2\pi x}{L}\right) + c_1x + c_2, \tag{8}$$

https://doi.org/10.1017/S0263574709005669 Published online by Cambridge University Press

where c_2 is an undetermined integration constant. Note that the deflection curve $v(x)$ in Eq. (8) contains five unknown quantities $\{a_0\ a_1\ a_2\ c_1\ c_2\}$. To determine the distributed moment that produces the deflection curve that is compatible with the given boundary conditions at the free end, we need to determine the unknown quantities using appropriate boundary conditions. Boundary conditions concerning the vertical and angular deflections at the fixed and free ends provide four equations that relate the five unknown quantities to each other. The cantilever beam has no vertical and angular deflections at the fixed end that leads to the following equations:

$$\left(\frac{\mathrm{d}v}{\mathrm{d}x}\right)_{x=0} = \frac{a_1 L}{2\pi} + c_1 = 0, \tag{9}$$

$$(v)_{x=0} = -\frac{a_2 L^2}{4\pi^2} + c_2 = 0. \tag{10}$$

Since the vertical and angular deflections at the free end are given, the following equations are obtained from the prescribed boundary conditions:

$$\phi_{\mathrm{F}} = \left(-\frac{\mathrm{d}v}{\mathrm{d}x}\right)_{x=L} = -\frac{a_0 L}{EI} + \frac{a_1 L}{2\pi EI} - \frac{c_1}{EI}, \tag{11}$$

$$\delta_{\mathrm{F}} = (-v)_{x=L} = -\frac{a_0 L^2}{2EI} + \frac{a_2 L^2}{4\pi^2 EI} - \frac{c_1 L}{EI} - \frac{c_2}{EI}. \tag{12}$$

Therefore, $\{a_0\ a_1\ a_2\ c_1\ c_2\}$ should be determined in such a way that Eqs. (9)–(12) are satisfied simultaneously. This task is accomplished by solving a linear system $\mathbf{Ay} = \mathbf{b}$ established in accordance with Eqs. (9)–(12) for $\mathbf{y} = [a_0\ a_1\ a_2\ c_1\ c_2]^T$.

Since the linear system $\mathbf{Ay} = \mathbf{b}$ contains more equations than the number of unknown quantities, the solution $\mathbf{y}$ is not unique.[24] This implies that there are multiple bending moment distributions that create the deflections compatible with the given boundary conditions. Note that we are seeking an optimal beam shape that is characterized by minimum strain energy. We need to identify one particular beam shape with minimum strain energy among those satisfying the given boundary conditions. In order to acquire the deflection curves that satisfy the given boundary condition, we determine a general solution to $\mathbf{Ay} = \mathbf{b}$ that consists of a homogeneous solution and a particular solution. The homogeneous solution $\mathbf{y}_{\mathrm{h}}$ to $\mathbf{Ay} = \mathbf{b}$ is determined by solving its null space problem $\mathbf{Ay}_{\mathrm{h}} = \mathbf{0}$. The solution to $\mathbf{Ay} = \mathbf{b}$ leads to its particular solution $\mathbf{y}_{\mathrm{p}}$. Therefore, the general solution to $\mathbf{Ay} = \mathbf{b}$ is obtained by superposing the homogeneous solution $\mathbf{y}_{\mathrm{h}}$ and the particular solution $\mathbf{y}_{\mathrm{p}}$.

$$\mathbf{y} = \mathbf{y}_{\mathrm{p}} + \mathbf{y}_{\mathrm{h}} = \begin{bmatrix} -\dfrac{EI\phi_{\mathrm{F}}}{L} \\ \dfrac{EI\pi}{L^2}(-2\delta_{\mathrm{F}} + L\phi_{\mathrm{F}}) \\ 0 \\ \dfrac{EI}{2L}(-2\delta_{\mathrm{F}} + L\phi_{\mathrm{F}}) \\ 0 \end{bmatrix} + \lambda \begin{bmatrix} 0 \\ 0 \\ \dfrac{4\pi^2}{L^2} \\ 0 \\ 1 \end{bmatrix}, \tag{13}$$

where $\lambda \in (-\infty, \infty) \subset \Re$. The general solution $\mathbf{y}$ in Eq. (13) implies that there are an infinite number of solutions to $\mathbf{Ay} = \mathbf{b}$ since any vectors from the null space of $\mathbf{A}$ to the particular solution $\mathbf{y}_{\mathrm{p}}$ is a solution to $\mathbf{Ay} = \mathbf{b}$. Substituting Eq. (13) into Eqs. (5) and (8), we can express the bending moment M_{b} and the deflection curve v as a function of λ.

Since we are concerned with a cantilever beam on a plane, the strain energy is determined solely by the curvature. According to the Euler–Bernoulli Beam theory, the strain energy (SE) is approximated in terms of the deflection v as follows:

$$\mathrm{SE} = \frac{1}{2}\int_0^L \frac{M_{\mathrm{b}}^2}{EI}\,\mathrm{d}x = \frac{EL}{2}\int_0^L \left(\frac{\mathrm{d}^2 v}{\mathrm{d}x^2}\right)^2 \mathrm{d}x. \tag{14}$$

Considering the bending moment is a function of λ, we can verify that the strain energy is also a function of the single variable λ following Eq. (14). In order for the beam to have minimum strain energy, the following stationary condition has to be satisfied:

$$\frac{\mathrm{d}\,\mathrm{SE}}{\mathrm{d}\lambda} = 0. \tag{15}$$

This optimality condition for strain energy SE in Eq. (14) allows us to determine a unique λ^*, for which the bending moment $M_{\mathrm{b}}(x)$ yields the deflection curve that has minimum strain energy as well as satisfies the prescribed boundary condition. From the optimality condition in Eq. (15), the following λ^* for minimum strain energy is obtained:

$$\lambda^* = 0. \tag{16}$$

The second derivative of strain energy verifies that SE is minimum for $\lambda = \lambda^*$.

$$\frac{\mathrm{d}^2\mathrm{SE}}{\mathrm{d}\lambda^2} = \frac{8\pi^4}{EIL^3} > 0 \tag{17}$$

Consequently, the analytical expression for an optimal cantilever beam can be obtained by substituting λ^* given in Eq. (16) into Eq. (8), and may be written as follows:

$$v_{\mathrm{opt}} = \frac{1}{4L\pi}\left[I^2(2\pi x(2\delta_{\mathrm{F}} + \phi_{\mathrm{F}}(x - L))) + L(L\phi_{\mathrm{F}} - 2\delta_{\mathrm{F}})\sin\left(\frac{2\pi x}{L}\right)\right]. \tag{18}$$

The cantilever beam with minimum strain energy in Eq. (18) is referred to as an optimal beam or an optimal beam model. The optimal beam model is capable of creating optimal beams for any boundary conditions imposed on the vertical deflection δ_{F} and the angular deflections ϕ_{F} at the free end.

It is straightforward to extend the aforementioned procedure for determining optimal plane curves to the cases using the Fourier series representation of $M_{\mathrm{b}}(x)$ with higher-order terms. When higher-order terms are included in Eq. (5), a more accurate representation of $M_{\mathrm{b}}(x)$ is possible, and hence the deflection curve v in Eq. (8) can describe plane curves with minimum deformation in a more precise manner. However, the higher-order terms added to Eq. (5) may lead

https://doi.org/10.1017/S0263574709005669 Published online by Cambridge University Press

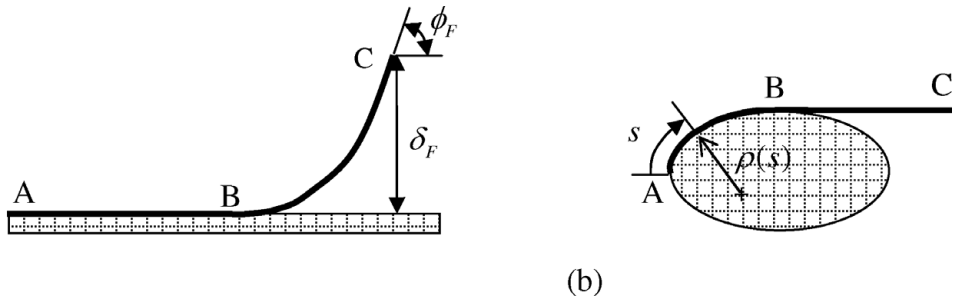

Fig. 2. Elastic linear objects in a continuous contact with a rigid surface; (a) elastic linear objects in contact with a flat surface; (b) elastic linear objects in contact with a curved surface.

to the increase in the dimension of the null space of **A**. The boundary conditions in Eqs. (9)–(12) provide four equations from which the coefficients in Eq. (5) and the integration constants in Eq. (8) can be determined. The number of unknown variables in the system $\mathbf{Ay} = \mathbf{b}$ increases, whereas the number of equations that enable determining the coefficients and integration constants is fixed. As a result, the linear system $\mathbf{Ay} = \mathbf{b}$ contains more unknown variables than the system established using $M_\mathrm{b}(x)$ in Eq. (5). The increase in the number of variables leads to the increase in the number of basis vectors that span the null space of **A**. Consequently, the optimal deflection curve in Eq. (8) and the strain energy in Eq. (14) become a function of multiple variables. Note that the bending moment and the strain energy are a function of the single variable λ when they are determined using the bending moment in Eq. (5). If the bending moment and the strain energy include multiple variables due to the higher-order terms added to Eq. (5), the stationary condition and the minimality of SE should be analysed on the basis of the Jacobian and Hessian matrices of **A**. Although such a high-order representation of $M_\mathrm{b}(x)$ could lead to more elaborate models for optimal plane curves, the analytical expression tends to be complicated and the complexity involved in the analysis tends to increase. Therefore, we decided to use $M_\mathrm{b}(x)$ in Eq. (5) to develop a simple analytical expression for optimal plane curves as it allows us to determine reasonably accurate optimal curves without intensive computation.

A drawback of the optimal beam model lies in the fact that it estimates only the vertical deflections of a beam. Since the Euler–Bernoulli beam theory is designed for beams with small deflections, it is also assumed that there are no changes in the horizontal coordinate L of the beam's end. However, if the beam undergoes large deflections, the horizontal deflections caused by flexural shortening are no longer negligible. In order to represent inextensible elastic linear object with large deformations, we adjust the horizontal coordinate of the free end in such a way that the beam maintains its initial length. In a two-dimensional space, the length of a deflection curve $v(x)$, $l(L)$, is written as follows:

$$l(L) = \int_0^L \sqrt{1 + \left(\frac{\mathrm{d}v}{\mathrm{d}x}\right)^2}\,\mathrm{d}x, \tag{19}$$

where L is the horizontal coordinate of the free end. The symbolic form of $l(L)$ is obtained from v_opt in Eq. (18). In order to determine the horizontal deflection that is compatible with the given length l_p, one may want to consider the following root-finding problem:

$$l(L) - l_p = 0. \tag{20}$$

Unfortunately, the algebraic expression for $l(L)$ is not available due to the complexity involved in the symbolic expression of the integrand of Eq. (19). Hence, we use the bisection search method to determine the horizontal coordinate L^* for the given length l_p. The bisection search method is an efficient root-finding algorithm that is suitable for a unimodal function such as $l(L)$.[22] The horizontal and vertical deflections of optimal curves of constant length can be efficiently decided for any prescribed boundary conditions at the free end in this manner.

The optimal beam model can be extended in order to represent elastic linear objects in a continuous contact with the surface of a rigid object. When an elastic linear object is tangent to the surface of a rigid object, the bending moment in the region in contact with the surface is determined by the curvature of the rigid surface according to the moment–curvature relationship in Eq. (4). For instance, let us consider the elastic linear object in Fig. 2(a). The segment AB is in continuous contact with the flat rigid surface. Therefore, the segment AB has zero curvature and the bending moment in the region AB is zero as well according to the moment–curvature relationship given in Eq. (4). Since the bending moment is constant in the region AB, the shear force is also zero. The deflections of the remaining curved segment BC can be determined on the basis of the optimal beam model. Since the curved segment BC should smoothly join with the segment AB, the angular deflection at point B must be zero. Therefore, the segment BC can be modelled as a cantilever beam. Then the deflections of the segment BC can be acquired using the optimal beam model for prescribed deflections at point C. Let us consider another example shown in Fig. 2(b). In Fig. 2(b), the elastic beam is bent around the curved rigid object. Since the elastic beam is in continuous contact with the curved rigid surface, its curvature is identical with that of the rigid surface. Then the bending moment in the segment AB is obtained from the curvature $\rho(s)$ of the rigid surface in accordance with the moment–curvature relationship given in Eq. (4). The segment BC can be modelled as a cantilever beam. The curvature of the beam at point B should be the same as that of the rigid surface

https://doi.org/10.1017/S0263574709005669 Published online by Cambridge University Press

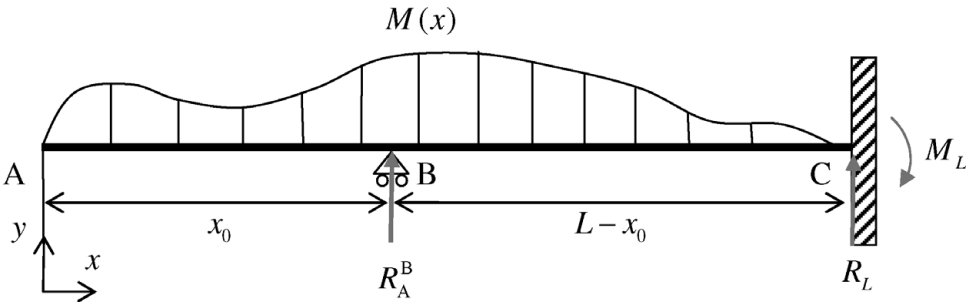

Fig. 3. An elastic beam with an overhang subjected to a distributed moment.

since there should be no abrupt changes in the curvature along the beam. Given the deflections at points B and C, the deflections of the segment BC can be decided by the optimal beam model. In this manner, we can replicate elastic linear objects in a continuous contact with a rigid surface using the optimal beam model.

3. Optimal Plane Curves in Contact with Rigid Objects

It is of interest to explore optimal curves in contact with rigid objects in order to utilize them for motion planning for elastic linear objects that may collide with obstacles. The motion of rigid bodies is usually designed such that their collision with obstacles is avoided. Unlike motion planning for rigid bodies, the contact between objects and obstacles sometimes needs consideration for efficient motion planning for flexible systems. If an elastic linear object travels through a narrow and complicated passage between obstacles, it is difficult to discover a continuous feasible path of the elastic object that does not collide with the obstacles. Even if a collision-free path is found, it will still be difficult to manipulate the object in a way that collision with the obstacles is completely avoided. It could be easy and convenient for us not only to plan the motion but also to manipulate the object when we take into account its contact with the obstacles and its sliding motion on the surface of the obstacles. On the other hand, it could be difficult to decide the points on the body that will be in contact with rigid obstacles before the contact occurs in planning the motion. However, considering it is preferable to maneuver the body following a collision-free path, the contact with the obstacle would be considered only when the collision-free path can hardly be discovered. If one encounters such circumstances, a collision-free path can be designed until the body gets in contact with the obstacle at prescribed points and plan the remaining path using the model that takes into account contacts with obstacles which will be presented in this section. We will discuss an analytical model for optimal beams in contact with rigid obstacles in this section.

One of the most common circumstances that the elastic linear object may experience would be the one in which it is in contact with obstacles at several points along the object. In order to represent an elastic linear object in contact with a rigid object, we are concerned with the beam with an overhang subjected to a distributed moment shown in Fig. 3. The roller support at point B represents the contact between the elastic object and the rigid object. To represent elastic linear objects in various shapes, we determine the deflection curve for various vertical and angular deflections at the free end. We assume that there is no friction between the beam and the roller support. The support of the roller located at distance x_0 from the free end develops the reaction $R_{\mathrm{A}}^{\mathrm{B}}$. The free-body diagram of the entire beam in Fig. 3 indicates that there are three unknown reactions; $R_{\mathrm{A}}^{\mathrm{B}}$, R_L and M_L. As there are only two available equations of equilibrium for moments and for vertical forces, the number of the unknown reactions exceeds the number of equations of equilibrium. Therefore, this system is statically indeterminate to the first degree. In order to determine the reaction forces in the statically indeterminate system, we will treat the reaction $R_{\mathrm{A}}^{\mathrm{B}}$ as an unknown quantity so that the remaining reactions, M_L and R_L, can be determined based on the statics of the system once $R_{\mathrm{A}}^{\mathrm{B}}$ is decided.

Since the bending moment changes abruptly due to the effect of the reaction $R_{\mathrm{A}}^{\mathrm{B}}$ at point B, the deflection of the beam should be analysed for two separate segments. In order to express the moment distribution in the most general manner, the bending moments $M_{\mathrm{b}}^{\mathrm{AB}}$ in segment AB and $M_{\mathrm{b}}^{\mathrm{BC}}$ in segment BC are expressed in terms of sine and cosine shape functions as follows:

$$M_{\mathrm{b}}^{\mathrm{AB}}(x) = a_1 \sin\left(\frac{2\pi x}{L}\right) + a_2 \cos\left(\frac{2\pi x}{L}\right), \quad (21a)$$

$$M_{\mathrm{b}}^{\mathrm{BC}}(x) = a_1 \sin\left(\frac{2\pi x}{L}\right) + a_2 \cos\left(\frac{2\pi x}{L}\right) + (x - x_0) R_{\mathrm{A}}^{\mathrm{B}}. \quad (21b)$$

In establishing the bending moments $M_{\mathrm{b}}^{\mathrm{AB}}$ and $M_{\mathrm{b}}^{\mathrm{BC}}$, we assume that the bending moment across the entire beam developed by the distributed moment $M(x)$ is given by $M_{\mathrm{b}}(x)$ in Eq. (5). $M_{\mathrm{b}}^{\mathrm{AB}}$ and $M_{\mathrm{b}}^{\mathrm{BC}}$ indicate the bending moment acting on segments AB and BC, respectively. Substituting the bending moments in Eqs. (21a) and (21b) into the moment curvature relationship in Eq. (4), we obtain the following second-order differential equations of the deflection curves v^{AB} for segment AB, and v^{BC} for segment BC:

$$EI \frac{\mathrm{d}^2 v^{\mathrm{AB}}}{\mathrm{d}x^2} = a_1 \sin\left(\frac{2\pi x}{L}\right) + a_2 \cos\left(\frac{2\pi x}{L}\right), \quad (22a)$$

$$EI \frac{\mathrm{d}^2 v^{\mathrm{BC}}}{\mathrm{d}x^2} = a_1 \sin\left(\frac{2\pi x}{L}\right) + a_2 \cos\left(\frac{2\pi x}{L}\right) + (x - x_0) R_{\mathrm{A}}^{\mathrm{B}}. \quad (22b)$$

https://doi.org/10.1017/S0263574709005669 Published online by Cambridge University Press

Integration of Eqs. (22a) and (22b) leads to the following equations that represent the angular deflection of the beam:

$$EI\frac{\mathrm{d}v^{\mathrm{AB}}}{\mathrm{d}x} = -a_1\left(\frac{L}{2\pi}\right)\cos\left(\frac{2\pi x}{L}\right) + a_2\left(\frac{L}{2\pi}\right)\sin\left(\frac{2\pi x}{L}\right) + c_1, \tag{23a}$$

$$EI\frac{\mathrm{d}v^{\mathrm{BC}}}{\mathrm{d}x} = -a_1\left(\frac{L}{2\pi}\right)\cos\left(\frac{2\pi x}{L}\right) + a_2\left(\frac{L}{2\pi}\right)\sin\left(\frac{2\pi x}{L}\right) + \left(\frac{x^2}{2} - x_0 x\right)R_{\mathrm{A}}^{\mathrm{B}} + c_2, \tag{23b}$$

where c_1 and c_2 are the constants of integration. The equations for the vertical deflection can be acquired by integrating Eqs. (23a) and (23b)

$$EIv^{\mathrm{AB}} = -a_1\left(\frac{L}{2\pi}\right)^2\sin\left(\frac{2\pi x}{L}\right) - a_2\left(\frac{L}{2\pi}\right)^2\cos\left(\frac{2\pi x}{L}\right) + c_1 x + c_3, \tag{24a}$$

$$EIv^{\mathrm{BC}} = -a_1\left(\frac{L}{2\pi}\right)^2\sin\left(\frac{2\pi x}{L}\right) - a_2\left(\frac{L}{2\pi}\right)^2\cos\left(\frac{2\pi x}{L}\right) + \frac{R_{\mathrm{A}}^{\mathrm{B}}}{6}x^3 - \frac{R_{\mathrm{A}}^{\mathrm{B}}x_0}{2}x^2 + c_2 x + c_4, \tag{24b}$$

where c_3 and c_4 are the constants of integration.

As shown in Eqs. (24a) and (24b), the integration of the differential equations (22a) and (22b) yields a total of four unknown constants of integration, c_1, c_2, c_3 and c_4. Because the coefficients of the shape functions, a_1 and a_2, in the bending moment and the reaction $R_{\mathrm{A}}^{\mathrm{B}}$ are also unknown quantities, this problem contains a total of seven unknown quantities. Therefore, we need seven conditions to determine the unknown quantities. The seven conditions can be acquired from boundary conditions and continuity conditions. The vertical and angular deflections are zero at the fixed end

$$\left(v^{\mathrm{BC}}\right)_{x=L} = -a_2\left(\frac{L}{2\pi}\right)^2 + \frac{R_{\mathrm{A}}^{\mathrm{B}}}{6}L^3 - \frac{R_{\mathrm{A}}^{\mathrm{B}}x_0L^2}{2} + c_2L + c_4 = 0, \tag{25}$$

$$\left(\frac{\mathrm{d}v^{\mathrm{BC}}}{\mathrm{d}x}\right)_{x=L} = -a_1\left(\frac{L}{2\pi}\right) - \left(\frac{L^2}{2} - x_0L\right)R_{\mathrm{A}}^{\mathrm{B}} + c_2 = 0. \tag{26}$$

The prescribed vertical and angular deflections at the free end lead to the following equations:

$$\delta_{\mathrm{F}} = \left(-v^{\mathrm{AB}}\right)_{x=0} = \frac{1}{EI}\left[a_2\left(\frac{L}{2\pi}\right)^2 - c_3\right], \tag{27}$$

$$\phi_{\mathrm{F}} = \left(-\frac{\mathrm{d}v^{\mathrm{AB}}}{\mathrm{d}x}\right)_{x=0} = \frac{1}{EI}\left[a_1\left(\frac{L}{2\pi}\right) - c_1\right], \tag{28}$$

where δ_{F} and ϕ_{F} denote vertical and angular deflections at the free end, respectively. The deflection at $x = x_0$ is assumed to be prescribed

$$\delta_{\mathrm{B}} = \left(-v^{\mathrm{AB}}\right)_{x=x_0} = a_1\left(\frac{L}{2\pi}\right)^2\sin\left(\frac{2\pi x_0}{L}\right) + a_2\left(\frac{L}{2\pi}\right)^2 \times \cos\left(\frac{2\pi x_0}{L}\right) - c_1x_0 + c_3, \tag{29}$$

where δ_{B} denotes the prescribed vertical position of the roller support at point B. The continuity conditions for the deflection curve stems from the fact that the deflection curve should be continuous at the point where the reaction force is acting. In order to satisfy the continuity of the deflection curve at point B, the vertical and angular deflections as determined for the left-hand part of the beam should be the same as those determined for the right-hand part of the beam.

$$\left[\frac{\mathrm{d}v^{\mathrm{AB}}}{\mathrm{d}x}\right]_{x=x_0^-} = \left[\frac{\mathrm{d}v^{\mathrm{BC}}}{\mathrm{d}x}\right]_{x=x_0^+} : c_1 - c_2 + \frac{x_0}{2}R_{\mathrm{A}}^{\mathrm{B}} = 0 \tag{30}$$

$$\left[v^{\mathrm{AB}}\right]_{x=x_0^-} = \left[v^{\mathrm{BC}}\right]_{x=x_0^+} : x_0c_1 + c_3 - x_0c_2 - c_4 + \frac{x_0^3}{3}R_{\mathrm{A}}^{\mathrm{B}} = 0 \tag{31}$$

The seven linear algebraic equations (25)–(31) are sufficient to determine the seven unknowns, $\mathbf{y} = \left[a_1\ a_2\ c_1\ c_2\ c_3\ c_4\ R_{\mathrm{A}}^{\mathrm{B}}\right]^T$. We can construct a linear system $\mathbf{Ay} = \mathbf{b}$ in accordance with Eqs. (25)–(31) in order to solve these equations simultaneously for $\mathbf{y}$. Note that the number of equations in $\mathbf{Ay} = \mathbf{b}$ is the same as the number of unknowns. Therefore, the unique deflection $\mathbf{y}$ can be decided in a deterministic way for a given boundary condition. For a cantilever beam without roller supports, an infinite number of beam deflections could be found for prescribed boundary conditions. Unlike those free cantilever beams, the beam with an overhang has only one unique equilibrium configuration, because only one deflection curve passes through the given contact point among those satisfying the prescribed boundary conditions.

4. Elastic Linear Objects in Contact with Multiple Obstacles

In this section, we will extend the analytical model for beams with an overhang in order to represent elastic linear objects in contact with multiple rigid objects. The optimal beam model to be discussed in this section replicates elastic linear objects that may collide with a number of rigid obstacles.

In order to represent elastic linear objects in contact with multiple rigid objects, we consider the cantilever beam with $N-1$ roller supports in Fig. 4. This beam is loaded by a distributed moment that creates a deflection curve that is compatible with prescribed deflections at the free end. The bending moment is expressed using sine and cosine shape functions in Eq. (21a). The $N-1$ supports develop reaction forces, $R_1^2, R_2^3, \ldots, R_i^{i+1}, \ldots, R_{N-1}^N$ where R_i^{i+1} denotes the reaction force between segments S_i and S_{i+1}. The free-body

https://doi.org/10.1017/S0263574709005669 Published online by Cambridge University Press

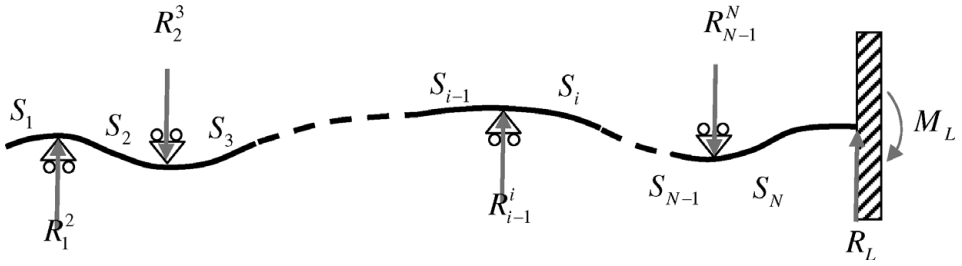

Fig. 4. A free-body diagram of a cantilever beam with $N-1$ roller supports.

diagram in Fig. 4 indicates that the vertical reaction force R_L and the reaction moment M_L are acting on the beam at the fixed end and hold the beam in equilibrium with the $N-1$ reaction forces. As there are only two available equations of equilibrium, this beam is statically indeterminate. In order to determine these unknown reaction forces and moments, we regard the reaction forces R_i^{i+1}, $i = 1, 2, \ldots, N-1$, as unknown quantities.

Apparently, the reaction forces acting on the beam give rise to abrupt changes in the bending moment. Therefore, the bending moment should be evaluated for segments between the reaction forces. Substituting the bending moments that are evaluated for each segment into the moment–curvature relationship in Eq. (4), we may obtain N differential equations from which the deflection curve can be acquired. Note that the beam consists of N segments. Then the deflection curve is determined by integrating these differential equations two times. Therefore, the algebraic equations for the deflection curve contain $2N$ integration constants. In addition to these integration constants and the reaction forces, we need to determine the coefficients of the shape functions, a_1 and a_2, that define the bending moment in the beam. Therefore, a total of $3N+1$ unknown quantities should be determined in order to obtain the deflection curve.

As was done for beams with an overhang, these unknown quantities can be determined using boundary and continuity conditions. The boundary conditions imposed on the angular and vertical deflections at the fixed end and the free end provide four conditions. The vertical deflections at the points where the roller supports are located may be assumed to be known without a loss of generality. The prescribed deflections at the contact points yield $N-1$ conditions. Since the continuity condition implies that the deflection curves determined for each segment should be continuous, the vertical and angular deflections at the points where the segments meet each other should also be continuous. Since the beam contains $N-1$ contact points, and two equations are established for each contact point, the continuity condition leads to a total of $2N-2$ conditions. Consequently, the boundary conditions and the continuity conditions provide a total of $3N+1$ conditions that exactly match the number of unknown quantities. In this way, the unique deflection curve of a cantilever beam in contact with $N-1$ rigid objects can be decided in a deterministic manner.

Moll and Kavraki[21] also modelled a spatial curve in contact with rigid objects. In order to make the problem tractable, they assumed that the slope at the points where the curve is in contact with the rigid object was given. Then optimal curves were acquired by minimizing the deformation energy for the curves between contact points. However, it is difficult to obtain globally optimal curves from such a curve model because the slope at contact points has to be determined such that the deformation energy of the entire curve is minimized.

5. Performance of the Optimal Beam Models

In this section, the performance of the optimal beam model is explored by examining its accuracy and practical applications. In Section 6.1, we verify the optimal beam model given in Eq. (18) by comparing it with closed-form solutions to Eq. (4) and the exact deflections of a cantilever beam with large deflections. The accuracy of the optimal beam model is investigated in comparison with the pseudo-rigid-body model. In order to explore the accuracy further, we compare the deflection curves determined using the optimal beam model with those acquired by minimizing the curvature energy in Eq. (1). The applications of the optimal beam model are demonstrated through several numerical simulations. Cantilever beams with several roller supports are presented in order to demonstrate how the optimal beams with roller supports represent elastic linear objects in contact with rigid objects. The inverse kinematics of hyper-redundant robots is solved for prescribed end-effector configurations using the optimal beam model. Finally, we demonstrate how the optimal beam model can be exploited as an efficient local path planner. The optimal motion of elastic linear objects between two given optimal plane curves will be planned using the optimal beam model.

5.1. Verification of the optimal beam models

In order to verify that the optimal beam model given in Eq. (18) identifies curves with minimum curvature energy, we compared the optimal beams with closed-form solutions to Eq. (4) that are available in classical solid mechanics text books.[6,8] The moment–curvature relationship depicted in Eq. (4) is for beams with small deflections. Hence, if the optimal beam contains only small displacements, its deflection curve should be identical to the closed-form solutions. Let us consider the cantilever beam with the concentrated moment M_0 and concentrated force P at the free end in Fig. 5(a). The vertical deflection v and angular deflection v' can be acquired by solving Eq. (4) for the moment M_0 and the force P[6,8]:

$$v = -\frac{M_0 x^2}{2EI} - \frac{Px^2}{6EI}(3L - x). \tag{32}$$

We assume that the beam has a unit length and a unit flexural rigidity EI without loss of generality. For the

https://doi.org/10.1017/S0263574709005669 Published online by Cambridge University Press

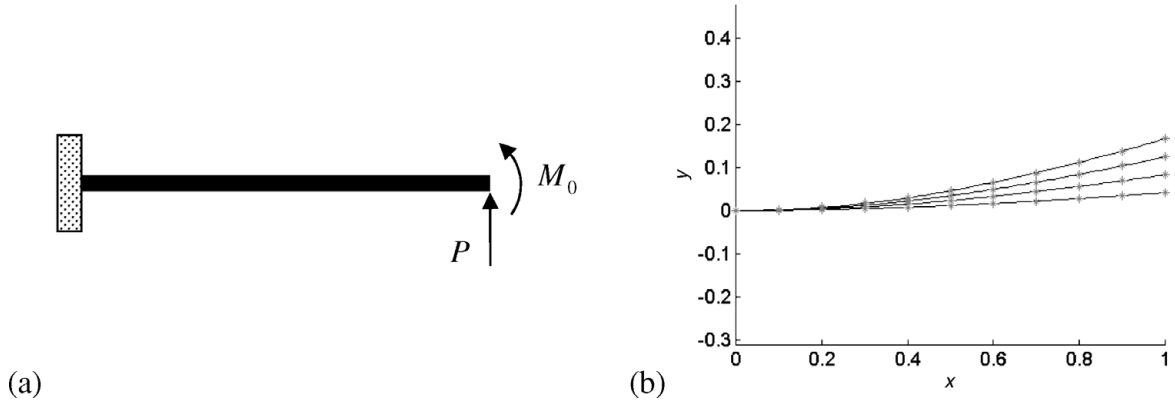

Fig. 5. (a) Cantilever subjected to a concentrated moment M_0 and a concentrated force P at the free end; (b) deflection curves determined for various M_0 and P. Solid lines represent optimal beams while the asterisks (*) represent the exact deflections of a cantilever beam following the Euler–Bernoulli beam model.

beam to have small deflections, the vertical and angular deflections in Eqs. (32a) and (32b) are determined for $M_0 = \{0.05\ 0.1\ 0.15\ 0.2\}^T$ and $P = \{0.05\ 0.1\ 0.15\ 0.2\}^T$. In order to ensure the deflections are small, the vertical deflections are expressed as a dimensionless quantity relative to the length of the beam L. The dimensionless vertical and angular deflections at the free end developed by M_0 and P are $\delta_F/L = \{0.0417\ 0.083\ 0.125\ 0.167\}^T$ and $\phi_F = \{0.075\ 0.15\ 0.225\ 0.3\}^T$ (rad), respectively. In this example, there are no changes in the horizontal coordinate of the free end because we are dealing with a cantilever beam with small deflections. In Fig. 5(b), each * represents the deflections determined by Eq. (32); On the other hand, the solid lines represent optimal beams where vertical and angular deflections at the free end are the same as those determined by the closed-form solution in Eq. (32). Figure 5(b) shows that the optimal beams are identical with the exact deflections obtained from Eq. (32). Hence, this example verifies that the optimal beam model in Eq. (18) not only captures the deflections for prescribed constraints imposed on the vertical and angular deflections at the free end but also produces curves with minimum curvature energy. Note that the deflection curves acquired from the moment–curvature relationship have minimum strain energy. Consequently, this result also confirms that the optimal beam model in Eq. (18) is valid for beams with small deflections and captures the beam deflections with minimum curvature energy that satisfy prescribed constraints imposed on the vertical and angular deflections at the free end.

The optimal beam model in Eq. (18) is derived from the Euler–Bernoulli beam model that is valid for beams with small deflections. If deflection curves need to be estimated for beams with large deflections, the optimal beam model in Eq. (18) becomes less accurate because when the beam undergoes large deflections, its horizontal deflection, due to flexural shortening, is no longer negligible. In order to take into account changes in the horizontal deflection, we adjust the horizontal deflection at the free end in such a way that the beam maintains constant length using Eq. (20). The verification of these optimal beams of constant length with large deflections is undertaken by comparing them with closed-form solutions developed for a cantilever beam with large deflections. Let us consider a cantilever beam with a concentrated force at the free end. When the cantilever beam undergoes large deflections, the horizontal deflection a and the vertical deflection b at the free end are expressed in terms of elliptic integrals.[11] In Fig. 6(a), the circles and solid lines represent the deflections acquired from the optimal beam model in Eq. (18). The exact deflection path following the elliptic-integral solution is represented by $+$. The deviation of the optimal beams from the elliptic-integral solution tends to occur as the beam undergoes large deflections. In order to explore the

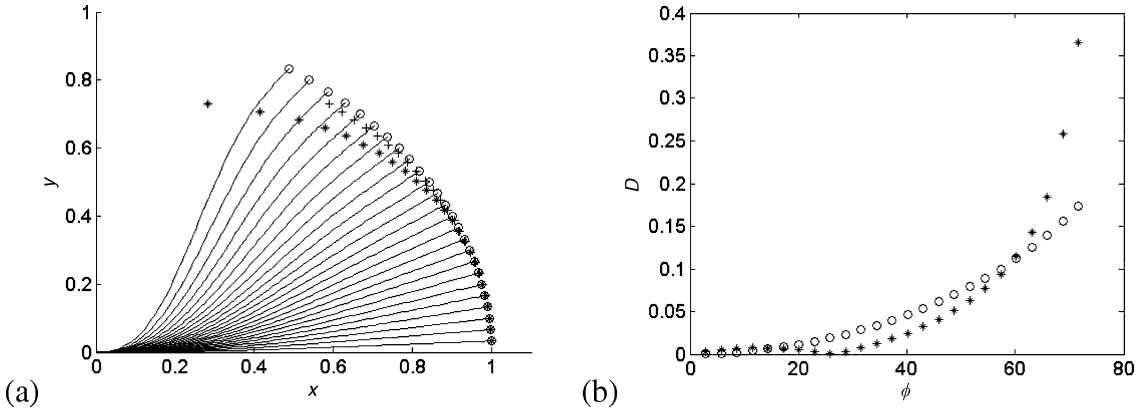

Fig. 6. (a) The deflections of a cantilever beam with a concentrated force at the free end; (b) the relative error versus the angular deflections at the free end.

https://doi.org/10.1017/S0263574709005669 Published online by Cambridge University Press

ranges in which the optimal beam model is valid, we examine the distance between the optimal beams and the elliptic-integral solution. The deflections of the optimal beam are represented by the distance between the free end of the deformed beam and that of the undeformed beam defined as follows:

$$\delta_o = \sqrt{(L-\alpha)^2 + \beta^2}, \tag{33}$$

where α and β denote the horizontal and vertical deflections at the free end, respectively. Analogously, the exact deflections following the elliptic-integral solution can be written as follows:

$$\delta_r = \sqrt{(L-a)^2 + b^2}. \tag{34}$$

Then, the accuracy of the optimal beam model can be analysed based on the following dimensionless error that is measured relative to the real deflections:

$$\frac{\text{Error}}{\delta_r} = \frac{\|\delta_r - \delta_o\|}{\delta_r}, \tag{35}$$

where $\|\delta_r - \delta_o\|$ represents the Euclidean distance between δ_r and δ_o.[20] Figure 6(b) shows that the relative error is just below 0.2 when the angular deflection at the free end is near 75°. The accuracy of the optimal beam model becomes apparent when the relative error of the optimal beam model is compared with that of the pseudo-rigid-body model.[11] The pseudo-rigid-body model estimates the deflections of a flexible beam based on an equivalent system composed of rigid bodies and torsional springs. In Fig. 6(a, b), the deflection path and the relative error acquired from the pseudo-rigid-body model are represented by the asterisks (*). The relative error almost reaches 0.4 when the angular deflection at the free end approaches 75°, which is greater than that of the optimal beam model. This error analysis result verifies that elastic beams with large deflections are better represented by the optimal beam model than by the conventional pseudo-rigid-body model.

The accuracy of the optimal beam model is explored further by comparing it with deflection curves determined by minimizing the curvature energy in Eq. (1). In order to acquire curves with minimum curvature energy, we are concerned with discretized curves acquired from the optimal beam model. It is difficult to determine optimal curves through such local optimization processes as the convergence to the optimal solution is not assured in general. However, if the curves obtained from the optimal beam model are used as an initial guess for the optimization, we can at least determine curves with lower curvature energy as those determined by the optimal beam model are located near true optimal solutions. Let us consider an optimal curve that is discretized with N nodes. These nodes are uniformly distributed along the curve and the position of the ith node is denoted by $\mathbf{r}_i = \{x_i, y_i\}, i = 1, 2, \ldots, N$. x_i and y_i indicate the x and y coordinates of the ith node $\mathbf{r}_i$, respectively. Then the curvature energy can be approximated by summing up the angles between adjacent line segments. The angle θ_i between the line segments $\mathbf{r}_{i,i-1} = \mathbf{r}_{i-1} - \mathbf{r}_i$ and $\mathbf{r}_{i,i+1} = \mathbf{r}_{i+1} - \mathbf{r}_i$

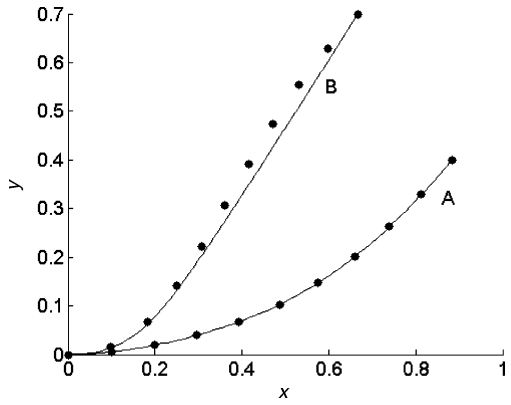

Fig. 7. Deflection curves acquired from the optimal beam model versus those determined through the minimization of curvature energy.

may be determined as follows:

$$\theta_i = \arccos\left[\frac{(\mathbf{r}_{i-1} - \mathbf{r}_i)\cdot(\mathbf{r}_{i+1} - \mathbf{r}_i)}{\|\mathbf{r}_{i-1} - \mathbf{r}_i\|\,\|\mathbf{r}_{i+1} - \mathbf{r}_i\|}\right] \quad \text{for} \quad i = 2, 3, \ldots, N-1. \tag{36}$$

Then we solve the following optimization problem in order to approximate optimal plane curves:

$$\underset{\{\theta_1,\theta_2,\ldots,\theta_N\}}{\text{Max}} \quad \sum_{i=1}^{N-2} \theta_i$$

Subject to

$$\phi_{\text{F}} = \frac{y_F - y_{N-1}}{x_F - x_{N-1}} \tag{37}$$

The equality constraint in Eq. (37) indicates that the endpoint of the curve should be compatible with the prescribed boundary condition imposed on the vertical and angular deflections at the free end. The position and slope at the endpoint, $\mathbf{r}_N = \{x_N, y_N\}$ should be $\{x_{\text{F}}, y_{\text{F}}\}$ and ϕ_{F}, respectively. The optimization was conducted for the optimal curves determined for $\{x_{\text{F}}, y_{\text{F}}, \phi_{\text{F}}\} = \{0.88, 0.4, \pi/3\}$ and $\{x_{\text{F}}, y_{\text{F}}, \phi_{\text{F}}\} = \{0.67, 0.7, \pi/3\}$. Line A in Fig. 7 represents the optimal curve determined for $\{x_{\text{F}}, y_{\text{F}}, \phi_{\text{F}}\} = \{0.88, 0.4, \pi/3\}$, and line B is determined for $\{x_{\text{F}}, y_{\text{F}}, \phi_{\text{F}}\} = \{0.67, 0.7, \pi/3\}$. The black dots in Fig. 7 represent optimal curves determined using the optimal beam model. As line A in Fig. 7 indicates, there is no discrepancy between the curve determined by solving Eq. (37) and the optimal beam as the curve undergoes small deflections. The curvature energy of line A is 0.8084 which is the same as that of the optimal beam represented by black dots (•). However, the difference between those curves is noticeable when they have large deflections as line B indicates. The curvature energy of line B in Fig. 7 is 1.2423 and that of the curve determined using the optimal beam model is 1.2084. The optimization allowed us to obtain a curve with lower curvature energy when it is conducted using the optimal beam as an initial guess. Note that it is usually difficult to obtain optimal solutions to Eq. (37) as long as the optimization is executed using local optimization methods. The approximation to the optimal

https://doi.org/10.1017/S0263574709005669 Published online by Cambridge University Press

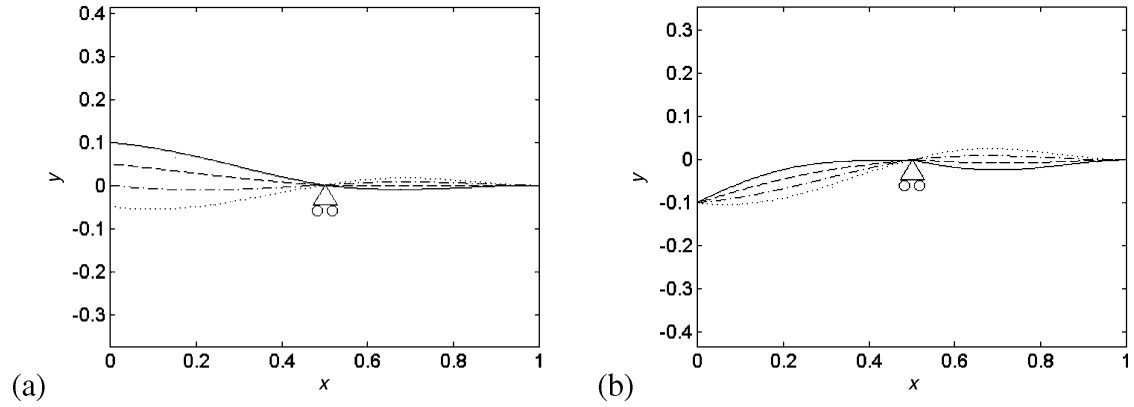

Fig. 8. The deflections of a cantilever beam with one roller support at $\{x, y\} = \{0.5, 0\}$. (a) The deflections determined for $\delta_F = \{0.05, 0, -0.05, -0.1\}^T$ and $\phi_F = 0.1$; (b) the deflections acquired for $\phi_F = \{-0.4, -0.2, 0, 0.2\}^T$ and $\delta_F = 0.1$.

plane curves shown in Fig. 7 could be accomplished only because the optimal beam model provided the initial guess. In addition, such optimization requires intensive computation in general as the problem contains a number of design variables. In contrast, the optimal beam model enables determining reasonably accurate optimal curves in an efficient manner.

5.2. Applications of the optimal beam models

The optimal beam model may have a wide range of practical applications. We will explore the potential applications through several examples that demonstrate how the model can be exploited to represent elastic linear objects in contact with rigid obstacles, to solve the inverse kinematics of hyper-redundant robots, and to plan the path of elastic linear objects.

As discussed in Section 3, the optimal beam model with roller supports is capable of representing elastic linear objects in contact with rigid objects. In order to acquire various elastic linear objects in contact with rigid obstacles, we determine the deflection curves for prescribed vertical and angular deflection at the free end and for the prescribed position of roller supports. Figure 8(a) shows optimal beams with a roller support positioned at $\{x, y\} = \{0.5, 0\}$ determined for various vertical deflections at the free end. The deflections with various angular deflections at the free end are also shown in Fig. 8(b). In order to represent elastic linear objects in contact with two rigid obstacles, the deflections of a cantilever beam supported by two roller supports are evaluated. The two roller supports in Fig. 9(a, b) are located at $\{x, y\} = \{0.2, 0.03\}$ and $\{x, y\} = \{0.6, -0.03\}$, respectively. The optimal beams in Fig. 9(a) are determined for various vertical deflections at the free end and Fig. 9(b) represents optimal curves determined for various angular deflections at the free end. Since these beams undergo small deflections, there are no horizontal deflections at the free end. As discussed in Section 5, the optimal beam model proposed in this paper allows us to plan the motion of elastic linear objects in contact with any number of rigid obstacles.

Chirikjian and Burdick[3] and Yim[29] represented a hyper-redundant robot using flexible curves in order to exploit the curves to identify the configuration of a hyper-redundant robot with an equivalent end-effector configuration. The fitting techniques developed by Andersson[1] and Fahimi *et al.*[7] enable determining the configuration of hyper-redundant robots for a given desired curve. The optimal beam model in Eq. (18) identifies extensible optimal plane curves for a given endpoint constraint with negligible computation and provides an efficient means of solving the inverse kinematics problem. Figure 10(a) exhibits optimal curves determined for various endpoint constraints using the optimal beam model. Note that, given the position and slope at the end point, the length of the curves in Fig. 10(a) is automatically adjusted according to Eq. (20). These curves can be used to determine the configuration of a hyper-redundant robot in a two-dimensional plane for prescribed

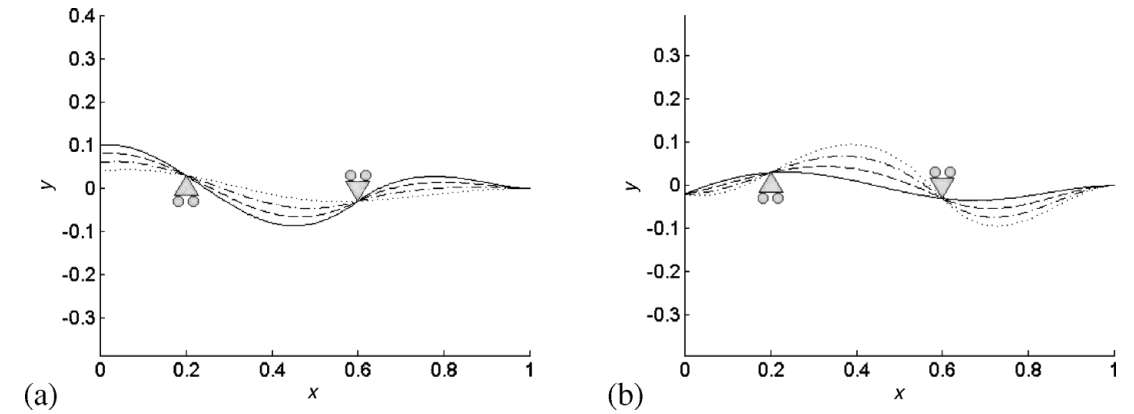

Fig. 9. The deflections of a cantilever beam with two roller supports. (a) The deflections determined for $\delta_F = \{-0.04, -0.06, -0.08, -0.1\}^T$ and $\phi_F = -0.1$ (rad); (b) the deflections acquired for $\phi_F = \{-0.4, -0.2, 0, 0.2\}^T$ (rad) and $\delta_F = 0.02$.

https://doi.org/10.1017/S0263574709005669 Published online by Cambridge University Press

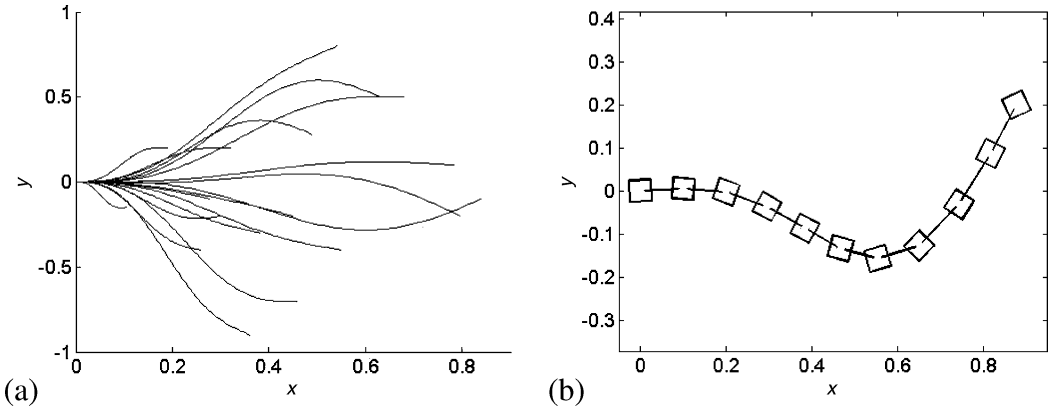

Fig. 10. (a) Optimal beams determined for various constraints imposed on the vertical and angular deflections at the free end and for various lengths of the beam; (b) a sequence of piecewise linear lines approximates a hyper-redundant modular robot that consists of 11 modules.

end-effector configurations. Figure 10(b) shows how a plane curve determined using the optimal beam model explore the inverse kinematics of a hyper-redundant robot that consists of 11 modules. In Fig. 10(b), a sequence of piecewise linear lines is acquired from a continuous optimal curve determined for the vertical deflection $\delta_F/L = 0.2$ and the angular deflection $\phi_F = 2.0$ at the free end. The squares in Fig. 10(b) represent the modules building the hyper-redundant robot. The configuration of these modular robots and the piecewise linear lines were determined following the fitting method proposed by Andersson.[1]

One of the most remarkable features of the optimal beam model is that efficient motion planning for elastic linear objects can be realized when the optimal beam model is incorporated into conventional motion planning algorithms[4,17,19] as a local path planner. Given two configurations, a local path planner determines intermediate configurations such that the object does not collide with obstacles. Unlike motion planning for a rigid-body, local path planning for elastic linear objects requires intensive computation if we utilize the conventional optimization-based method.[19,21] In contrast, the computational demand involved in evaluating intermediate configurations based on the following local path planning method is negligible compared to the optimization-based methods.

The motion of a cantilever beam is divided into two components; a rigid-body transformation and a deformation. In order to describe the deformation of the cantilever, a local coordinate frame $\{x, y\}$ is attached to the beam as shown in Fig. 11(a). The optimal deflection curve is uniquely determined for the prescribed vertical deflection δ_F and angular deflection ϕ_F at the free end. On the other hand, the rigid body transformation of the cantilever is defined by the position and orientation of the local frame $\{x, y\}$ relative to the space-fixed reference coordinate frame $\{X, Y\}$ in Fig. 11(a). The orientation and position of the local frame $\{x, y\}$ are denoted by $\{x_0, y_0\}$ and θ_0, respectively. Therefore, the configuration of the cantilever beam is entirely expressed by five parameters $\mathbf{q} = \{x_0, y_0, \theta_0, \delta_F, \phi_F\}$. Given the initial configuration $\mathbf{q}_i$ and the final configuration $\mathbf{q}_f$, the local path planner determines the intermediate configurations $\mathbf{q}_m$ between $\mathbf{q}_i$ and $\mathbf{q}_f$ by linearly interpolating the values of the parameters as follows:

$$\mathbf{q}_m = \mathbf{q}_i + t(\mathbf{q}_f - \mathbf{q}_i) \quad \text{for} \quad t \in [0, 1] \subset \Re. \tag{38}$$

Then the intermediate optimal configuration $\mathbf{q}_m$ is uniquely determined for the intermediate parameters using the optimal beam model. Figure 11(b) shows the motion of an elastic linear object planned using the optimal beam model. The two solid lines in Fig. 11(b) represent the initial and final configurations. The intermediate configurations represented by the dashed lines are determined for the parameters that are uniformly sampled in accordance with Eq. (38).

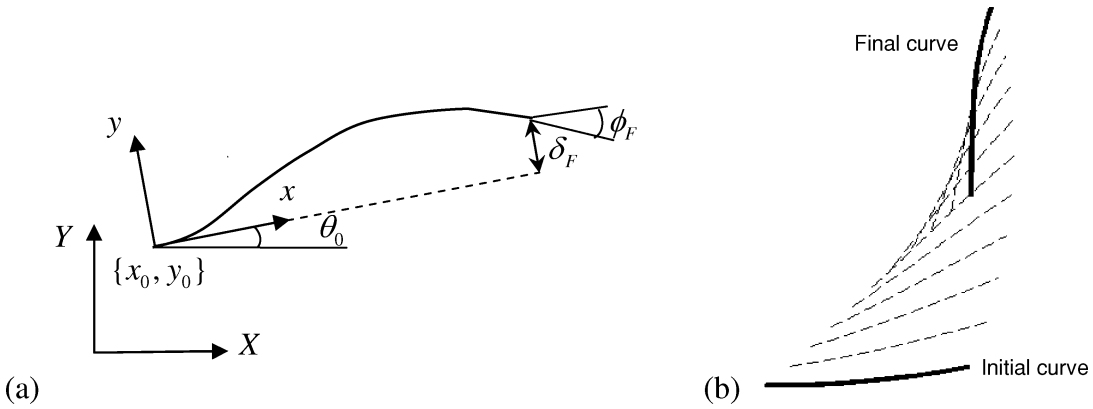

Fig. 11. (a) A cantilever beam expressed in a local coordinate frame attached to the beam; (b) local motion planning for elastic linear objects using the optimal beam model.

https://doi.org/10.1017/S0263574709005669 Published online by Cambridge University Press

The conventional local path planning method performs optimization in order to determine the optimal intermediate configurations, which entail intensive computation. Whereas, the optimal beam model provides optimal configurations using the analytical expression in Eq. (18), which explains why the motion planning based on the optimal beam model is more efficient than the conventional techniques.

The optimal beam model may also be applied to global path planning for elastic linear objects. Unlike the aforementioned local path planning algorithm, the trajectory of the fixed end is important in designing the global path for given initial and final configurations. Once the trajectory of the fixed end is decided, the entire global path can be decided with the help of the aforementioned local path planning algorithm. The trajectory of the fixed end may be planned using any conventional path planning algorithms such as the probabilistic road-map method,[17] the artificial potential field method[2] and the rapid-exploring random trees.[14] Using the optimal beam model, it is not difficult to compute all admissible configurations that do not intersect with rigid obstacles. Therefore, the configuration at each step of the trajectory may be determined so as to reduce the deformation of elastic linear objects during the motion.

6. Conclusion

The deflections of a cantilever beam loaded by a distributed moment have been determined for prescribed boundary conditions at the free end in order to replicate elastic linear objects in equilibrium or flexible plane curves with minimum deformation. We developed the optimal beam model to provide an analytical expression for optimal plane curves. Since the computational demand involved in calculating the deflections using the optimal beam model is negligible, efficient local path planning for elastic objects can be realized. The optimal path between two given optimal configurations was planned using the analytical optimal beam model. In order to plan the motion of elastic linear objects that may collide with multiple rigid obstacles, we explored a cantilever beam supported by multiple roller supports. The analytical expressions for the deflections provide a convenient and efficient means of replicating elastic linear objects in contact with multiple rigid objects.

The verification of the optimal beam model was accomplished in comparison with the pseudo-rigid-body model. We verified that the optimal beam model better represent beams with large deflections than the pseudo-rigid-body model. Since the optimal beam model is developed on the basis of the Euler–Bernoulli theory, the optimal deflections deviate from the exact deflections as the beam undergoes large deflections. However, in practice, the deformation of elastic objects is limited if the objects are manipulated within its elastic region. Therefore, the optimal beam model may be an accurate tool for motion planning for elastic objects that are manipulated within the elastic region. If the object is so flexible that it may experience large elastic deformations and an accurate estimation of the large deformation is required, one may want to employ the conventional optimization-based method using the optimal beams as an initial guess to acquire more accurate optimal plane curves.

We would also like to stress the following strengths of the optimal beam models over the conventional models. First, the optimal beam model supplies optimal curves with reasonable accuracy in a deterministic manner. All existing numerical methods possess the possibility of obtaining a curve corresponding to the local minimum of the curvature energy. Second, the optimal beam model creates extensible optimal plane curves for any prescribed endpoint constraints. The length of the optimal curve is adjusted automatically such that the given endpoint configuration becomes feasible. Finally, the analytical optimal beam model identifies optimal plane curves in contact with rigid objects where its curvature energy is globally minimum. The slopes of the curve at the contact points are decided so as to minimize the curvature energy of the entire curve.

The optimal beam model represents two-dimensional curves with minimum deformations. Hence, it is useful for motion planning for elastic linear objects or one-dimensional flexible systems manipulated on a plane. The inverse kinematics of a hyper-redundant robot operated on a plane can also be explored using the optimal beam model and the fitting techniques developed by Andersson[1] and Fahimi *et al.*[7]. If we employ the conventional computational models to determine plane optimal curves, computational expenses involved in determining the optimal curves become demanding. In contrast, the optimal beam model creates optimal plane curves without intensive computation in a deterministic manner as the optimal curves are computed on the basis of the analytical expressions for optimal plane curves. The efficiency of the optimal beam model in solving the inverse kinematics problem has been verified through several numerical simulations in which the configuration is determined using the fitting technique proposed by Andersson.[1]

Efficient path planning for flexible linear objects is also feasible as the path may be constructed so as to reduce the deformations along the path. In the future, we will explore global path planning algorithms based on the optimal beam model that realize convenient and efficient path planning for flexible objects. Although we have developed the optimal beam model for motion planning for elastic objects, it can also be applied to the animation of any flexible linear object that might collide with rigid objects.

Acknowledgements

This work was funded in part by a grant from the Natural Sciences and Engineering Research Council (NSERC) of Canada and the Canadian Space Agency.

References

1. S. B. Andersson, "Discretization of a continuous curve," *IEEE Trans. Rob.* **24**(2), 456–461 (2008).
2. J. Barraquand, B. Langlois and J. C. Latombe, "Numerical potential field techniques for robot path planning," *IEEE Trans. Syst. Man Cybernet.* **22**(2), 224–241 (1992).
3. G. S. Chirikjian and J. W. Burdick, "Kinematically optimal hyper-redundant manipulator configurations,"*IEEE Trans. Rob. Automat.* **11**(6), 794–806 (1995).
4. H. Choset, K. M. Lynch, S. Hutchinson, G. Kantor, W. Burgard, L. E. Kavraki and S. Thrun, *Principles of Robot Motion: Theory, Algorithms, and Implementations*. MIT Press, Cambridge, USA (2005).

https://doi.org/10.1017/S0263574709005669 Published online by Cambridge University Press

5. B. D. Coleman, I. Tobias and D. Swigon, "Theory of the influence of end conditions on self-contact in DNA loops," *J. Chem. Phys.* **103**(20), 9101–9109 (1995).
6. S. H. Crandall, N. C. Dahl and T. J. Lardner, *An Introduction to the Mechanics of Solids* (McGraw-Hill, New York, 1978).
7. F. H. Fahimi, H. Ashrafiuon and C. Nataraj, "An improved inverse kinematic and velocity solution for spatial hyper-redundant robots," *IEEE Trans. Rob. Automat.* **18**(1), 103–107 (2002).
8. J. M. Gere, *Mechanics of Materials*, 5th ed. (Brooks/Cole, CA, 2000).
9. K. G. Gopalakrishnan and K. Goldberg, "D-space and deform closure grasps of deformable parts," *Int. J. Rob. Res.* **24**(11), 899–910 (2005).
10. B. K. P. Horn, "The curve of least energy," *ACM Trans. Math. Software* **9**(4), 441–460 (1983).
11. L. Howell, *Compliant Mechanisms* (Wiley, New York, 2001).
12. E. Jou and W. Han, "Minimal-energy splines with various end constraints," In: Hagen, H. (ed.): *Curve and Surface Design*, 23–40, SIAM, Philadelphia, USA (1992).
13. A. M. Ladd and L. E. Kavraki, "Using motion planning for knot untangling," *Int. J. Rob. Res.* **23**(7–8), 797–808 (2004).
14. J. J. Kuffner and S. M. LaValle, RRT-Connect: An efficient approach to single-query path planning. In *Proc.IEEE Int'l Conf. on Robotics and Automation* (ICRA' 2000), 995–1001, San Francisco, CA, April (2000).
15. M. Kallay, "Plane curves of minimal energy," *ACM Trans. Math. Software* **12**(3), 219–222 (1986).
16. M. Kallay, "Method to approximate the space curve of least energy and prescribed length," *Comp.-Aided Des.* **19**(2), 73–76 (1987).
17. L. E. Kavraki, P. Švestka, J.-C. Latombe and M. H. Overmars, "Probabilistic roadmaps for path planning in high-dimensional configuration spaces," *IEEE Trans. Rob. Automat.* **12**(4), 566–580 (1996).
18. J. S. Kim and G. S. Chirikjian, "Conformational analysis of stiff chiral polymers with end-constraints," *Mol. Simul.* **32**(14), 1139–1154 (2006).
19. F. Lamiraux and L. E. Kavraki, "Planning paths for elastic objects under manipulation constraints," *Int. J. Rob. Res.* **20**(3), 188–208 (2001).
20. J. E. Marsden and M. J. Hoffman, *Elementary Classical Analysis* (W. H. Freeman and Company, New York, 1993).
21. M. Moll and L. E. Kavraki, "Path planning for deformable linear objects," *IEEE Trans. Rob.* **22**(4), 625–636 (2006).
22. P. Papalambros and D. J. Wilde, *Principles of Optimal Design* (Cambridge University Press, Cambridge, UK, 2000).
23. A. Remede and D. Henrich, "Direct and Inverse Simulation of Deformable Linear Objects," **In**: *Robot Manipulation of Deformable Objects*, ser. Advanced Manufacturing Series (D. Henrich and H. Wörn, eds.) (Springer Verlag, Berlin, Heidelberg, New York, 2000) pp. 43–70.
24. G. Strang, *Linear Algebra and Its Applications* (Harcourt Brace Jovanovich College Publishers, Orlando, FL, 1988).
25. D. Swigon, B. D. Coleman and I. Tobias, "The elastic rod model for DNA and its application to the tertiary structure of DNA minicircles in mononucleosomes," *Biophys. J.* **74**, 2515–2530 (1998).
26. S. P. Timoshenko and D. H. Young, *Engineering Mechanics*, 3rd ed. (McGraw-Hill, New York, 1951).
27. H. Wakamatsu and S. Hirai, "Static modeling of linear object deformation based on differential geometry," *Int. J. Rob. Res.* **23** (3), 293–311 (2004).
28. H. Wakamatsu, E. Arai and S. Hirai, "Knotting/unknotting manipulation of deformable linear objects," *Int. J. Rob. Res.* **25**(4), 371–395 (2006).
29. M. Yim, Locomotion with a Unit Modular Reconfigurable Robot *Ph.D. Thesis* (Department of Mechanical Engineering, Stanford University, Palo Alto, CA, 1994).

https://doi.org/10.1017/S0263574709005669 Published online by Cambridge University Press